# Time-Resolved PIV Measurements of Vortical Structures in the Upper Human Airways

Sebastian Große, Wolfgang Schröder, and Michael Klaas

Institute of Aerodynamics, RWTH Aachen University, D-52062 Aachen, Germany
s.grosse@aia.rwth-aachen.de

**Abstract.** A detailed knowledge of the three-dimensional flow structures in the human lung is an inevitable prerequisite to optimize respiratory-assist devices. To achieve this goal the indepth analysis of the flow field that evolves during normal breathing conditions is indispensable. This study focuses on the experimental investigation of the steady and oscillatory flow in the first lung bifurcation of a three-dimensional realistic transparent silicone lung model. The particle image velocimetry technique was used for the measurements. To match the refractive index of the model, the fluid was a mixture of water and glycerine. The flow structures occurring in the first bifurcation during steady inflow have been studied in detail at different flow rates and Reynolds numbers ranging from $\mathrm{Re_D} = 1250$ to $\mathrm{Re_D} = 1700$ based on the hydraulic diameter $D$ of the trachea. The results evidence a highly three-dimensional and asymmetric character of the velocity field in the upper human airways, in which the influence of the asymmetric geometry of the realistic lung model plays a significant role for the development of the flow field in the respiratory system. The inspiration flow shows large zones with secondary vortical flow structures with reduced streamwise velocity near the outer walls of the bifurcation and regions of high-speed fluid in the vicinity of the inner side walls of the bifurcation. Depending on the local geometry of the lung these zones extend to the next generation of the airway system, resulting in a strong impact on the flow-rate distribution in the different branches of the lung. During expiration small zones of reduced streamwise velocity can be observed mainly in the trachea and the flow profile is characterized by typical jet-like structures and an M-shaped velocity profile. To investigate the temporal evolution of the flow phenomena in the first lung bifurcation time-resolved recordings were performed for Womersley numbers $\alpha$ ranging from 3.3 to 5.8 and Reynolds numbers of $\mathrm{Re_D} = 1050$, 1400, and 2100. The results evidence a region with two embedded counterrotating vortices in the left bronchia. Furthermore, the measurements reveal a strong shear layer in the bronchia that evolves when the flow direction changes from inspiration to expiration. Due to the high intricacy of the natural lung geometry most research has been performed in simplified bifurcation models such that no comparably realistic and detailed experimental study of the flow field within the first bifurcation of the upper human airways has been presented as yet.

A. Schroeder, C. E. Willert (Eds.): Particle Image Velocimetry,
Topics Appl. Physics **112**, 35–53 (2008)

## 1 Introduction

The lung as the human respiratory organ consists of a repeatedly bifurcating network of tubes with progressively decreasing diameters. The understanding of the highly unsteady and nonlinear flow field within these tubes is of great importance to interpret particle-deposition patterns and thus to develop aerosol drug-delivery systems [1–5]. Furthermore, utilizability and efficiency of artificial lung ventilation highly depends on the velocity and pressure distribution, both of which are associated with a specific ventilation strategy. Despite numerous experimental and numerical investigations having been conducted so far it has to be stated that there still exists a considerable amount of uncertainty concerning the very complex flow field in the human lung. This is mainly due to the high intricacy of the human lung geometry. In other words, results for realistic models of the lung are still rare. The majority of experimental and numerical investigations has been performed using models with a simplified geometry, which might lead to flow fields that deviate considerably from realistic lung flows. For this reason, results could often not explain the fluid-mechanical causes for certain particle-deposition patterns or nonlinear lung-flow phenomena.

One of the earliest publications by *Schroter* and *Sudlow* [6] focused on velocity profiles and flow patterns in symmetric bifurcating geometries. The authors used hot-wire probes and smoke visualization techniques assuming a steady air flow in rigid tubes with smooth surfaces. These assumptions are commonly made with reference to the existing local Reynolds number based on the mean geometry diameters in the range of $\mathrm{Re_D} = 500$ to 2000 and Womersley numbers of about 5 to 25, which are typical values for normal breathing conditions. As far as the influence of the Reynolds number on the characteristics of the flow structures during inspiration is concerned, *Martonen* et al. [7] as well as *Grotberg* [8] report a strong dependence of the flow field on the Reynolds number in the Reynolds number ranges of $\mathrm{Re} = 200$ to 2000 and $\mathrm{Re} = 200$ to 1200, respectively. On the other hand, *Liu* et al. [9] found comparable flow patterns by numerically investigating an asymmetric human lung airway system for Reynolds numbers between 400 and 1600. Furthermore, there is no common consensus on the impact of the entry flow profiles on the flow structures evolving in the upper lung. While some investigators report the bifurcation-flow phenomena to be independent of the inflow conditions, *Yang* et al. [10] report a strong impact of different inflow conditions on the flow in the subsequent bifurcation zones. Since the flow between consecutive bifurcation regions cannot fully develop in a natural lung geometry, the upstream condition within the network of bifurcations influences the flow structures further downstream. Nevertheless, a large number of investigations have been performed for artificial geometries with rather long branches between subsequent bifurcations.

Experimental investigations of *Ramuzat* and *Riethmuller* [11] concentrated on a plane symmetric model of subsequent pipe bifurcations, hence in-

troducing a major simplification of the model geometry. In their experiments, oscillating flow phenomena have been investigated for different Womersley numbers, emphasizing the temporal development of the velocity through successive bifurcations and the quasisteadiness of the flow for low oscillation frequencies.

Recent numerical calculations focused on the analysis of aerosol transport and particle-disposition patterns and have been carried out by numerous groups, e.g., [12] and [13]. *Comer* et al. [1–3] investigated the flow structure in symmetric double bifurcations under steady conditions in a system consisting of three subsequent bifurcations. The Reynolds number based on the pipe diameter varied from $\mathrm{Re_D} = 500$ to 2000. The authors detected strong vortical flow fields especially in the region of the second bifurcation, leading to complex particle distributions and deposition patterns. The flow in a plane and nonsymmetric bifurcation has been calculated by *Liu* et al. [9]. Their simulations comprised the flow field from the fifth to the eleventh branch of the model of *Weibel* [14] resulting in Reynolds numbers in the range of $\mathrm{Re_D} = 200$ to 1600. All the aforementioned models were based on the planar character of the pipe network. Furthermore, most of the studies were performed for highly symmetric models with bifurcations that divide the lower generations' pipe into two subsequent tubular pipes with nearly or exactly likewise diameter.

Recently, experimental and numerical studies have been carried out for nonplanar lung geometries. *Caro* et al. [15] investigated steady inspiratory flow in a symmetric model of the lung with two generations. For planar and nonplanar configurations the results emphasized the different development of the flow fields and volumetric distributions between varying types of geometry. The distribution of the wall-shear stress in the different generations of the bronchia was measured by optically visualizing the reaction between acid vapor and blue litmus coatings in the bronchial system. It was concluded that inspiratory flow in larger human bronchial airways is asymmetric and swirling with implications for all transport processes including those of particles. A similar model has been used in a numerical simulation by *Comer* et al. [1]. The findings show that for the out-of-plane configuration of the different generations of the bronchia the particle-deposition patterns differed from the planar case and possessed higher particle efficiencies for diluted suspensions of inhaled particles where the efficiency is defined as the number of particles deposited in a certain section divided through the total number of particles entering the region.

Numerical results for the most complicated and realistic model of the lung geometry have been presented by van *Ertbruggen* et al. [16]. The results evidenced the highly three-dimensional character of the flow field, emphasizing the importance of nonfully developed flows in the branches due to the relatively short lengths.

Recent particle image velocimetry measurements in a realistic lung model by *Brücker* and *Schröder* [17] revealed large separation zones near the outer

wall of the bronchia during inspiration but did not evidence any separation regions during expiration.

The findings in the literature show that physically relevant studies of the bronchial airway anatomy and the corresponding flow field require realistic and thus complex models of the lung geometry. On the one hand, this challenge can be pursued by defining an artificial lung model with high complexity, taking into account the three-dimensional characteristics of the branches, e.g., asymmetry of the bifurcation zones, the "natural" ratio between the cross sections of subsequent generations of branches, the noncircular shape of real bronchia, and the impact of the upstream flow conditions on the mass-flow distributions in subbranches. On the other hand, a realistic lung model can be derived from original, hence exact, lung-geometry data. Modern clinical image-recording techniques allow the exact determination of the lung-geometry at least for the first six to ten bronchial branches. This offers the possibility to manufacture a "negative" kernel of the human airways made from solvable materials, which can be used to generate transparent silicone models ("positive"). This approach finally leads to a realistic model of the human lung providing optical access to the airways. The difficulty in such "natural" models is the lack of symmetry and orientation such that a fully three-dimensional investigation of the flow field is a must to adequately describe the flow structures.

The objective of this study is to perform detailed velocity measurements in the first bifurcation of such a realistic lung model using standard and time-resolved particle image velocimetry (PIV). The first experiments allow us to analyze the flow patterns in the first bifurcation of the human lung consisting of the trachea and the first bronchia generation. Steady inspiration and expiration flows have been studied for a variety of Reynolds numbers based on the trachea diameter D ranging from $\mathrm{Re_D} = 1250$ to 1700. Since the model extends to the 6th generation the effect of upstream bifurcations on the expiration flow can be investigated. Additionally, oscillating flow with Reynolds numbers ranging from $\mathrm{Re_D} = 1050$ to 2100 and Womersley numbers $\alpha$ ranging from 3.3 to 5.8, where the Womersley number is defined as $\alpha = 0.5 \cdot D \cdot \sqrt{2 \cdot \pi \cdot f/\nu}$, was investigated. Herein, the quantity $D$ denotes the diameter of the trachea, $f$ is the frequency of the ventilation cycles, and $\nu$ represents the kinematic viscosity of the fluid. The time-resolved measurements have been performed in a center plane in the first bifurcation region of the lung geometry, such that the temporal evolution of the flow field in the first lung bifurcation during a complete breathing cycle could be investigated.

In the following sections, first the experimental setup is described in great detail. Then, the results for steady and time-dependent flows are discussed. Finally, some conclusions conclude this chapter.

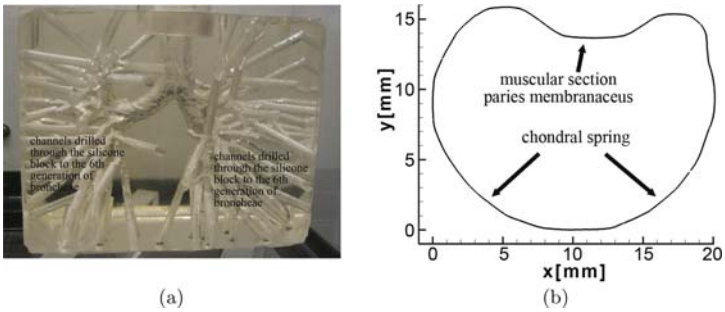


**Fig. 1.** (**a**) Picture of the hollow-lung model in silicone. (**b**) Sketch of the cross section of the trachea (plane normal to the average direction of the trachea, oriented 25.0° to the $z$-direction from Fig. 2)

## 2 Experimental Setup

### 2.1 Lung Model

The PIV experiments were conducted in a realistic, three-dimensional lung model that extends to the 6th generation of the bronchial system. It is fabricated from transparent silicone (RTV815) to allow perfect optical access. Figure 1 depicts a picture of the hollow lung model in the silicone block. The complete lung geometry is indicated in Fig. 2 by showing several cross sections.

At inspiration, the fluid enters the lung model through an anatomically shaped trachea as illustrated in Fig. 1. The flow exits the model through channels that have been drilled from the 6th generation's endings through the block sides. The trachea of the model possesses the typical shape of a natural trachea with a dorsal indentation. The real human trachea is stiffened by chondral springs in the ventral part of the cross section. The dorsal, i.e., the back part of the trachea consists of a muscular structure (paries membranaceus) and allows a widening of the trachea.

### 2.2 In- and Outflow Conditions

The choice of an appropriate inflow condition is crucial for the investigation of the lung flow since the velocity profile in the trachea has a strong impact on the flow field in the first lung bifurcation [10]. To enable a comparison with numerical results and with future computations a defined inflow condition in the trachea was chosen. Most numerical calculations use a classical fully developed laminar profile as the inflow condition. Also, parallel flow profiles have been investigated. To uniquely define the inflow characteristics and to ensure a fully developed velocity profile, an $L = 500\,\mathrm{mm}$ long pipe section with a constant cross section matching that in the upper part of the trachea was modeled. The hydraulic diameter in the model $D$ is approximately

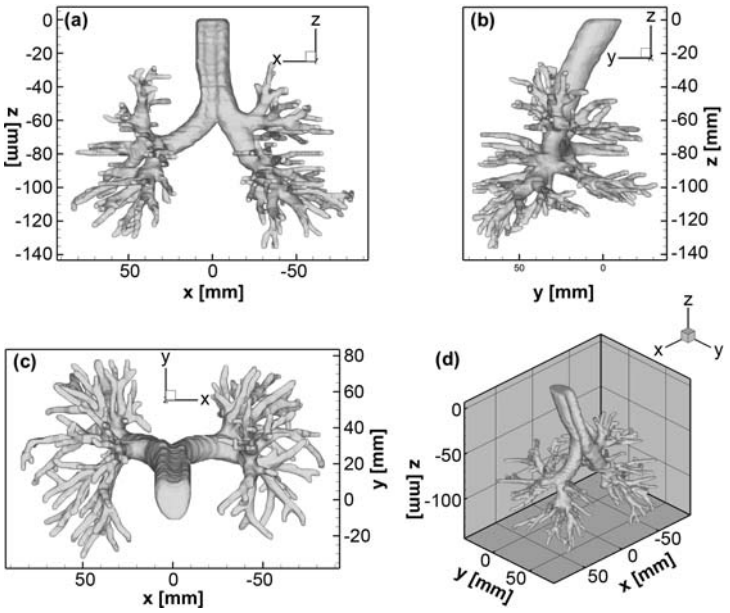


**Fig. 2.** Illustrations of the realistic lung model. (**a**) dorsal or back view, (**b**) lateral view, and (**c**) caudal or top view; (**d**) isometric view

18.3 mm leading to a ratio of $L/D = 27$. The Reynolds number based on the hydraulic diameter of the trachea ranges from $\mathrm{Re_D} = 1250$ to 1700 for the steady-flow experiments. This results in a fully developed laminar profile at the inlet. Choosing an anatomically shaped trachea instead of a plain pipe flow helps to prevent flow separation in the lung inflow region by avoiding the discontinuous change of the cross section at the junction between the inflow pipe section and the trachea. At any rate, such a geometry would generate unphysical disturbances of the flow field further downstream of the bifurcations.

Note, the human trachea possesses a total length of 10–12 cm, measured from the laryngeal region (cartilage cricoidea) to the first bifurcation (bifurcatio tracheae). Hence, the flow entering the bifurcation will be strongly influenced by the geometry of the upper airways and the perturbations caused by the larynx region. Thus, the real flow in the human body cannot be considered fully developed.

The flow exits into a net of pipes, which have the same diameter as the branches of the 6th generation of the lung model. They were drilled into the silicone block such that they can be considered straight extensions of these branches. Due to the fact that the vertical pressure in the tank complies with the hydrostatic pressure distribution it can be assumed that the outlet pressure in the experiment is nearly constant for all branches of the 6th generation exiting into the tank.

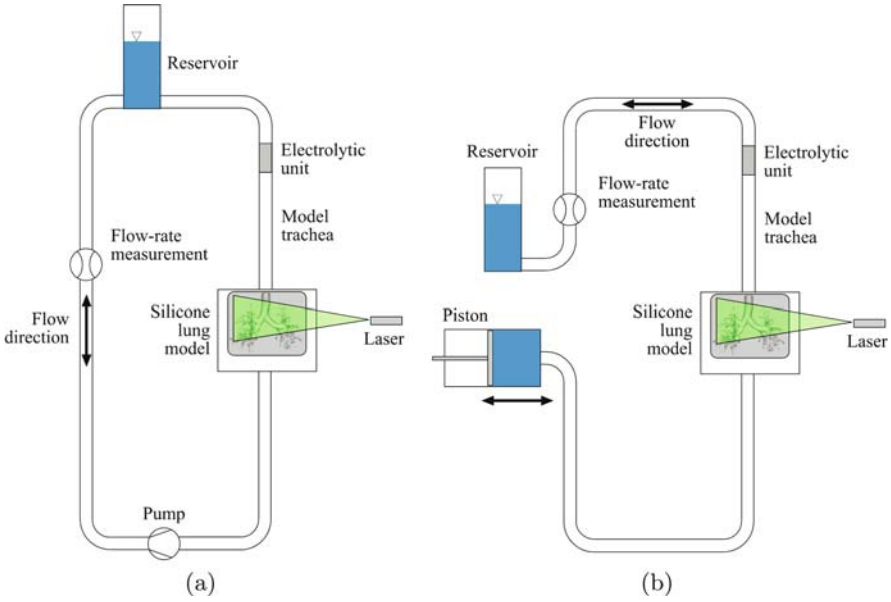


**Fig. 3.** (**a**) Schematic of the experimental setup for steady flow. (**b**) Schematic of the experimental setup for oscillating flow

Measurements at steady inspiration and expiration have been performed using a closed-circuit flow facility. Note that the experimental setup is identical for both cases except for the flow direction. For either setup the fluid supply for the tank has to be carefully positioned since a homogeneous flow circulation has to be guaranteed for an idealized flow distribution in the lung model. Measurements at oscillating flow, which were designed to simulate a breathing cycle, have been conducted with an open-circuit flow facility. In this case, a sinusoidal fluid movement was realized using a piston driven by an eccentrically supported rod. Figures 3a,b show schematics of the experimental setup for steady and oscillatory flow.

### 2.3 Flow Parameters

A water/glycerine mixture with a refractive index of $n = 1.44$, being identical to that of the silicone block, was used as flow medium. The dynamic viscosity of the mixture with 60.7 mass per cent glycerine is $\eta = 10.3 \times 10^{-3}\,\mathrm{Pa \cdot s}$ and the density $\rho = 1.153 \times 10^3\,\mathrm{kg/m^3}$ for the temperature during the experiments.

The Reynolds number $\mathrm{Re_D}$ for the steady-flow measurements was varied between 1250 and 1700. The Reynolds number $\mathrm{Re_D}$ for oscillatory flow based on the maximum flow velocity during inspiration was varied between 1050

**Table 1.** Flow parameters

| Parameter | Multi-plane | Steady inspiration | Steady expiration | Oscillating flow |
|---|---|---|---|---|
| Reynolds number $Re_D$ | 1700 | 1250–1700 | 1250–1700 | 1050–2100 |
| Mean trachea bulk velocity $U_{mean}$ (m/s) | 0.83 | 0.60–0.83 | 0.60–0.83 | – |
| Maximum trachea bulk velocity $U_{max}$ (m/s) | – | – | – | 0.50–1.10 |
| Womersley number $\alpha$ | 0 | 0 | 0 | 3.27–5.77 |
| Volumetric flow per cycle $V$ ($cm^3$) | – | – | – | 90.6–570 |
| Frequency (cycles/min) | – | – | – | 10.85–34.5 |

and 2100. The Womersley number range was 3.3 to 5.8. Hence, typical human breathing cycles under normal conditions can be simulated with this setup. A list of characteristic flow parameters of the different measurements is given in Table 1.

### 2.4 Tracer Particles

Hydrogen bubbles generated in an electrolytic unit upstream of the trachea were used as tracer particles. Since the amount of bubbles in plain water/glycerine is rather low due to missing electrolytes in the fluid a very small amount of saline additive is mixed into the fluid. The electrolytic unit was especially designed to avoid flow disturbances upstream of the trachea.

The size of the tracer particles depends on the electrolytic voltage, the distance between the metal cathode and anode of the electrolytic unit, and the mean flow velocity through the unit. The distance and voltage were adjusted to achieve an optimized size of the bubbles of 1–5 µm. Due to the laminar flow in the trachea it was necessary to start the electrolytic unit at least 5 min prior to the measurement series to generate a homogeneous distribution of particles. At very low Reynolds numbers it was necessary to switch off the unit during the measurements since bubbles were not torn off the metal surfaces by the low flow velocities but accumulated at the edges of the unit yielding tracer particles that were too large.

The use of hydrogen bubbles was necessary since standard flow particles (PA, etc.) led to heavy particle deposition on the walls of the lung model resulting in strong reflections at the boundaries of the bronchial system and as such in a significantly reduced quality of the images. However, first experiments done with solid particles showed flow structures comparable to those measured with hydrogen bubbles. Nevertheless, the use of solid tracer particles and hence the contamination of the model led to a considerably higher

number of invalid vectors in the measured velocity fields. The lifespan of the bubbles is in the range of 5–10 min such that for expiration the electrolytic unit could be kept in the same position in the flow circuit still ensuring a sufficient number of bubbles for the PIV measurements under reversed flow conditions.

### 2.5 Measurement Equipment and Image Evaluation

In all measurements a standard PIV system was used consisting of a double-cavity Minilite Nd:YAG laser with a nominal power of 25 mJ, a PCO Sensi-Cam QE double-shutter camera with a resolution of $1376 \times 1040$ px, and a lens with $f\# = 1.8$ to reduce the depth of focus to a minimum and to maximize the available light. To gain some first knowledge of the spatial evolution of the flow field in the first bifurcation during steady inspiration, experiments were performed at a Reynolds number of $\mathrm{Re_D} = 1700$ using a set of parallel lightsheets with a spacing of 1 mm and a field of view of $95.8 \times 72.4$ mm. Next, 500 images were taken at a frequency of 2 Hz for steady inspiratory and expiratory flow in a streamwise-oriented central plane of the bifurcation. The field of view for these measurements was approximately $74.6 \times 56.4$ mm. Based upon these results the temporal development of the flow structures in the left bronchia was investigated in detail with time-resolved PIV at a frame rate of 8 Hz and a field of view of approximately $72.4 \times 27.7$ mm. In this case 200 images were taken for each set of Womersley and Reynolds number. Thus, depending on the specific parameter combination a minimum of 4 to 14 complete inspiration and expiration cycles per experiment were captured.

The data was postprocessed using the commercial VidPIV 4.6 PIV software by ILA GmbH. A multipass correlation was applied starting with a $64 \times 64$ px interrogation size with 50 % overlap followed by an adaptive cross-correlation with a final $16 \times 16$ px interrogation window size leading to a vector spacing of 0.7 mm for the time-resolved measurements. Thus, approximately 25 vectors across the diameter of the first generation of bronchia could be achieved. Only weak local reflections from the walls allowed us to exactly determine the bronchial structure.

The dynamic range in the PIV images was up to 4096 grayscales and 4–6 particles per interrogation area led to a high accuracy of the adaptive correlation routines. Due to an achievable subpixel accuracy of less than 0.02 px of the routines under these conditions the accuracy in the velocity determination was better than 0.5 %. To determine the pulse distance at oscillating flow was rather difficult since the setting must be adapted to maximum inspiration or expiration flow velocities as well as to the quasistatic conditions at flow reversal.

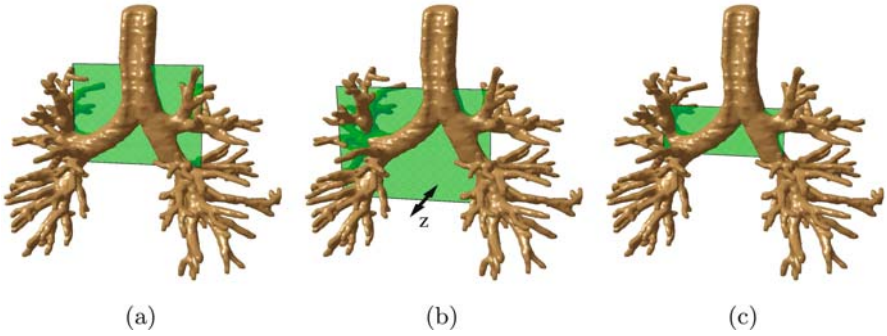


**Fig. 4.** Measurement planes in dorsal view for (**a**) multiplane measurements (only one plane is illustrated), (**b**) steady, and (**c**) oscillating flows

## 3 Results

To obtain some knowledge about the global structure of the flow field in the bifurcation of the trachea and bronchia, the first experiments were performed for steady inspiration at a constant Reynolds number of $\mathrm{Re_D} = 1700$. Due to the complexity of the velocity field in the bifurcation region the flow was recorded in thirteen parallel, vertical lightsheets with a lateral displacement of 1 mm, hence covering the complete cross section of the bronchia. This allowed the reconstruction of three-dimensional flow phenomena from the two-dimensional velocity distributions. Based on the results of these measurements, experiments were conducted for steady inspiration and expiration at two different Reynolds numbers of $\mathrm{Re_D} = 1250$ and $\mathrm{Re_D} = 1700$ to determine the influence of the Reynolds number on the flow field. To investigate the temporal and spatial evolution of the flow structures during a breathing cycle measurements were performed for a set of combinations of Reynolds number $\mathrm{Re_D}$ and Womersley number $\alpha$. The analysis of the data showed the impact of these parameters on the characteristics of the flow in the bifurcation region. The oscillating flow was generated by imposing a sinusoidal flow rate with zero mean velocity as described in Sect. 2.

Figure 4 illustrates the positions and sizes of the measurement planes with respect to the lung geometry for all cases investigated. The definitions “left” and “right” used in the following discussion of the findings are defined for the dorsal view on the upper human airways complying with the usual notation in anatomy.

### 3.1 Multiplane Measurements

Figure 5 illustrates the two-dimensional velocity distributions in the first bifurcation during steady inspiration at a Reynolds number $\mathrm{Re_D} = 1700$ in

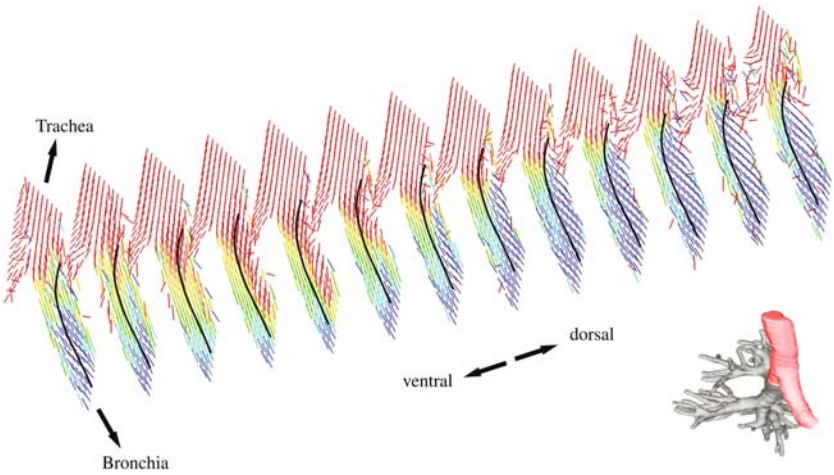


**Fig. 5.** Two-dimensional velocity distributions in the first bifurcation during steady inspiration at a Reynolds number of $Re_D = 1700$ in parallel planes. Vector color qualitatively emphasizes $u/w$. The *black line* represents the extension of the region containing the counterrotating vortices

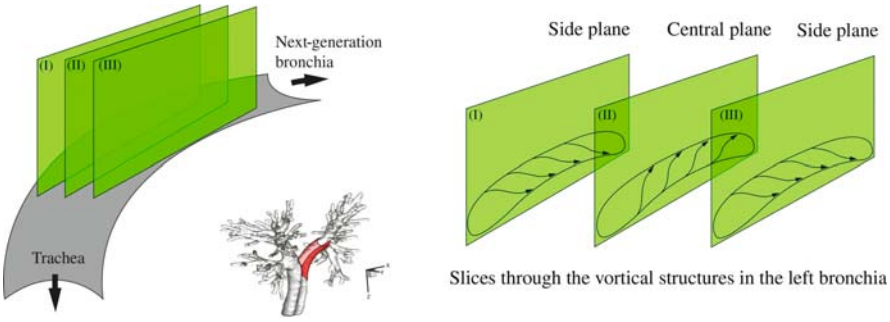


**Fig. 6.** Schematic of the two-dimensional measurement planes in the first bifurcation at three distinct positions

parallel planes. The vector fields evidence a zone with a strongly reduced streamwise velocity component at the upper wall of the left bronchia, which is slightly skewed in the ventral direction. This asymmetry results most likely from the angle between the central planes of the trachea and bronchia and hence from the torsion of mother and daughter branches of the bifurcation.

Since the terminus "separation" usually denotes a region containing reversed flow, it can not be applied to describe the flow structure identified in the measurements. Although the mean streamwise velocity is strongly reduced within these regions and especially near the side walls, no flow recir-

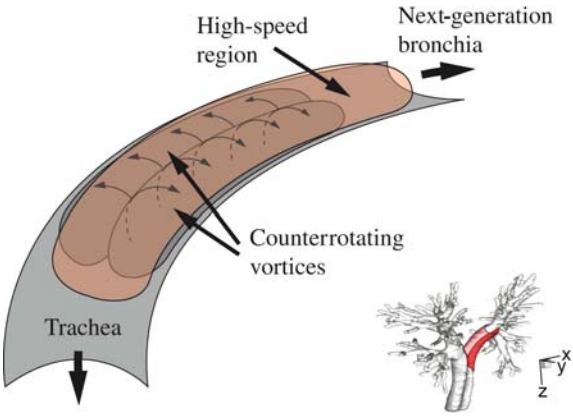


**Fig. 7.** Schematic of the two counterrotating vortices evolving along the outer bifurcation. The high-speed region is illustrated in *red*

culation could be evidenced. Since the measurement planes cover the whole cross section of the bronchia the three-dimensional shape of the region of secondary flow structures can be determined. The complete flow pattern is depicted in Figs. 6 and 7. The measurements indicate that two counterrotating vortices form inside the region of reduced velocity. The fluid flows along the outer walls of the bronchia to the central plane and then to the centerline towards the high-speed region on the inner curve of the bifurcation. This fluid motion is superposed with fluid transport in the downstream direction generating a spiral-like shape of the vortices. The multiplane measurements also reveal that the measurements only in the central plane allow the reconstruction of the spatial extent of the counterrotating vortices with sufficient accuracy.

### 3.2 Steady Inspiration and Expiration

Figures 8a,b show a smooth laminar velocity profile from the trachea entering the bifurcation zone at inspiration. The figures illustrate the velocity magnitude and some velocity profiles for selected positions in the bifurcation, which evidence a large zone of strongly reduced velocity in the left bronchia and strongly skewed velocity distributions. This area is located at the inner curve of the bifurcation and extends to the bronchia centerline. As discussed above, two counterrotating vortices exist in this region. These secondary flow phenomena resemble spiral-like structures moving the fluid from the center of the bronchia sidewards to the upper wall of the bifurcation and back to the central region of the bronchia. The fluid captured in these vortical structures is still transported along the bronchia, but with a reduced mean volumetric flow rate. This causes the remaining flow to form a jet-like high-speed region along the lower curve of the bifurcation.

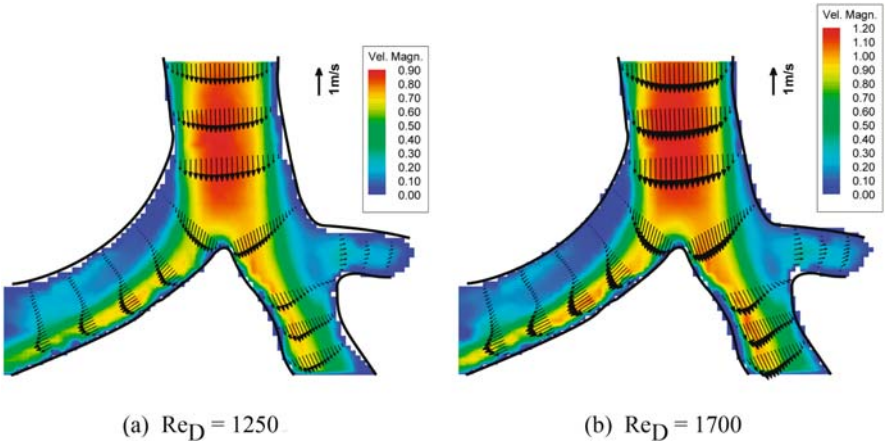


**Fig. 8.** Velocity profiles at different positions for steady inspiration flow with $Re_D = 1250$ and $Re_D = 1700$. Contour levels show the vector magnitude

Figure 9 shows the instantaneous flow pattern evidencing the transport of the fluid in the center plane. A schematic of the overall flow structure in the left bronchia illustrating the counterrotating vortices was already depicted in Fig. 7. As a consequence of the high velocities near the lower wall of the bifurcation a strong shear layer evolves. A similar behavior can be observed in the right bronchia, although the intensity and extension of the corresponding region is less marked compared to that in the left bronchia. This is caused by the smaller angle of deflection of the right bronchia. Regarding the mass-flow distribution at steady inspiration the geometry leads to an unbalanced distribution, i.e., the volume flux in the right lung lobe is larger than in the left lobe.

Figure 10 shows the velocity magnitude and velocity profiles at selected positions for steady expiration. The flow is strongly characterized by the inlet velocity from the subbranches. The velocity profiles in the bronchia possess an M-like shape resulting from the merging fluid jets of the corresponding subbranches. Due to this effect, the flow cannot develop a parabolic velocity profile but rather possesses a two-peak velocity distribution in the radial direction. This velocity profile represents the inflow condition for the next junction during expiration. The flow following the inner curves possesses higher peak values of the velocity magnitude such that a skewed M-form of the velocity profiles develops. Figure 10 also indicates two small regions in the trachea where the fluid cannot follow the extremely strongly curved wall. Here, the fluid is displaced towards the centerline of the trachea where the peak velocity values occur.

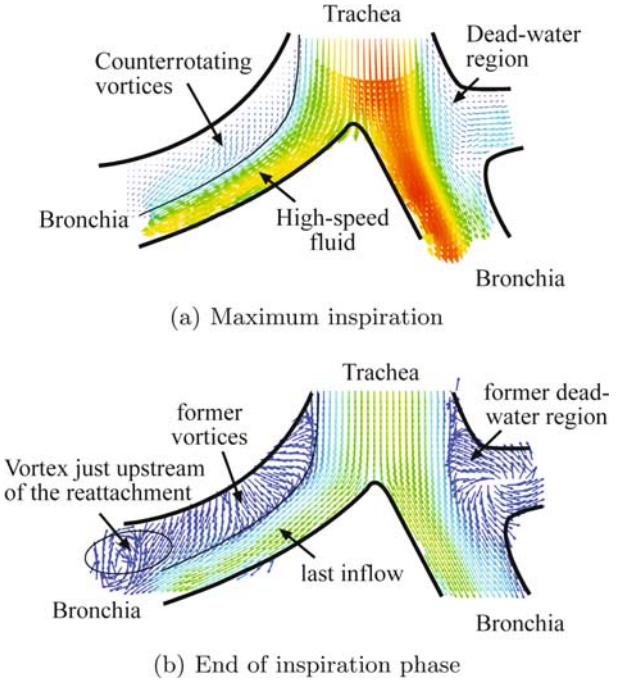


**Fig. 9.** Flow structure in the center plane of the first bifurcation. (**a**) Vector length and color show the velocity magnitude. (**b**) Vectors possess a uniform length, contours show the velocity magnitude

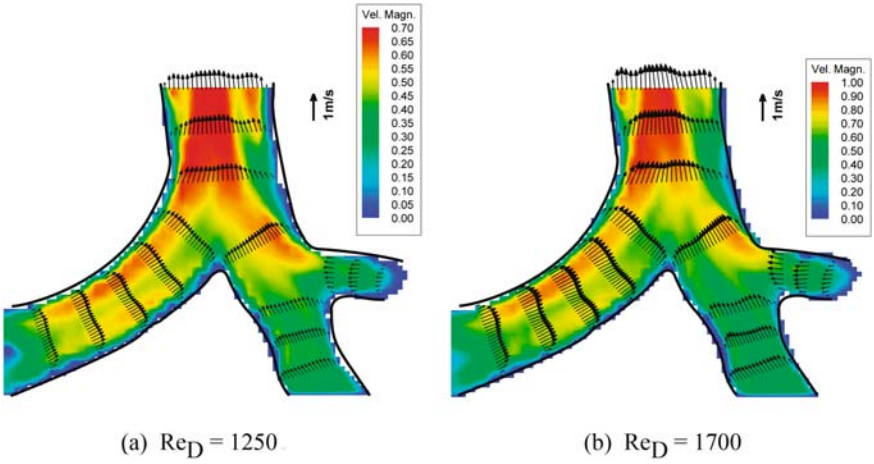


**Fig. 10.** Velocity profiles at different positions for steady expiration at $Re_D = 1250$ and $Re_D = 1700$. Contours show the velocity magnitude

**Table 2.** Investigated parameter combinations of Reynolds number $Re_D$ and Womersley number $\alpha$

| Reynolds no. $Re_D$ (−) | Womersley no. $\alpha$ (−) | Frequency $F$ (cycles/min) | Volumetric flow $V$ ($cm^3$) |
|---|---|---|---|
| 1050 | 3.27 | 10.9 | 282.6 |
| 1400 | 3.27 | 11.0 | 376.8 |
| 2100 | 3.27 | 10.85 | 565.0 |
| 1050 | 4.70 | 22.1 | 136.3 |
| 1400 | 4.70 | 22.3 | 181.8 |
| 2100 | 4.70 | 22.9 | 272.6 |
| 1050 | 5.77 | 34.5 | 90.6 |
| 1400 | 5.77 | 33.2 | 120.8 |
| 2100 | 5.77 | 33.5 | 181.2 |

### 3.3 Oscillating Flow

Oscillating flow measurements have been conducted for a set of parameter combinations of Reynolds number $Re_D$ and Womersley number $\alpha$, which are summarized in Table 2. The Reynolds number is based on the maximum bulk velocity at inspiration.

In this phase the Reynolds number increases continuously until it reaches its peak value at 25 % of the breathing cycle. When the Reynolds numbers exceeds a critical level of roughly $Re_D = 800$ to 1000, the vortical flow structures described in Sect. 3.1 occur in the bronchia. While this region is fed by the near-wall fluid from the trachea, the center fluid from the trachea flows straight through the bifurcation and is split at its inner radius (bifurcatio tracheae) following the lower bronchial contour in small streaks of high-speed fluid. At the lower end of the two counterrotating vortices, i.e., nearly three bronchia diameters downstream of the bifurcation, a strong vortical structure can be identified that increases in size and strength when inspiration comes to its end (Fig. 9). Before expiration starts, the region in which the counterrotating vortices existed begins to roll up from the lower end of the bronchia generating a strong shear layer between the already reversed flow near the outer bifurcation wall and the remaining inflow of the former high-speed zone. Finally, the latter region is completely suppressed and expiration sets in. In the right bronchia, a dead-water region reaches even over the next-generation branch. Here, strong vortical structures can also be identified during the reversal of the flow direction.

During expiration the flow field in the bifurcation and the trachea is strongly influenced by the upstream flow conditions. Neither separation zones nor a dead-water region as found during inspiration can be observed. Only downstream of the trachea does a moderate dead-water region form on the outer walls.

Figure 11 illustrates the time-dependent evolution of the out-of-plane vorticity distribution in the central plane in the region of the first bifurcation for $\mathrm{Re_D} = 2100$ and $\alpha = 3.27$. Herein, the vorticity component is defined as $\omega_y = \frac{\partial u}{\partial z} - \frac{\partial w}{\partial x}$, where $u$ is the horizontal and $w$ the vertical velocity component, and $x$ and $z$ are the corresponding cartesian coordinates in the measurement plane.

The illustration of the temporal evolution of the vorticity evidences the spatial extent of the vortical structures during inspiration and expiration by visualizing the shear layer that lies between the vortical flow structures in the bifurcation and the remaining high-speed jet. During inspiration, narrow bands of increased vorticity illustrate the extension of the vortices in the left and right bronchia. As mentioned above, at expiration small dead-water zones can be found in the trachea. Due to an additional mass flow coming from the upper bronchial branch in the right lobe and due to a more pronounced curvature at the wall the secondary structures on the right side of the trachea are stronger than their counterpart on the left side. This can also be clearly observed in Figs. 10a,b. In Fig. 11, i.e., at maximum expiration, a centered region of high vorticity is evidenced in the left bronchia. This shear layer results from the merging jets of the two corresponding subbranches. Furthermore, the results show that, depending on the phase in the flow cycle, the vortical structures along the upper bifurcation wall change strongly in shape and size for low Reynolds numbers. Nevertheless, it can be stated that for Reynolds numbers over approximately $\mathrm{Re_D} = 1000$ the counterrotating vortices show the same extension for all investigated cases.

## 4 Conclusion and Outlook

Velocity measurements of steady inspiration and expiration at two Reynolds numbers of $\mathrm{Re_D} = 1250$ and $\mathrm{Re_D} = 1700$ were presented. The results evidenced the Reynolds number of the flow to play a minor role for the extension of the flow phenomena. For both Reynolds numbers during steady inspiration, very similar flow structures could be observed. To be more precise, the size of the counterrotating vortical structures did not depend on the Reynolds number as long as this Reynolds numbers stays above a critical level of roughly $\mathrm{Re_D} = 800$ to 1000. For the lower Reynolds numbers achieved during the oscillating flow studies the size of the evolving secondary flow structures depends rather strongly on the momentary Reynolds number. A highly intricate flow structure consisting of a spiral-like trajectory was found in a region along the upper wall of the left branch of the first bifurcation. From the presented results it can be clearly concluded that the characteristic length of the bronchial generations is too short to achieve fully developed flow profiles before entering the next generation of bronchia. Therefore, special care has to be taken when flow-rate distributions in this highly complex geometry are to be determined without having determined a complete 3D-3C velocity distri-

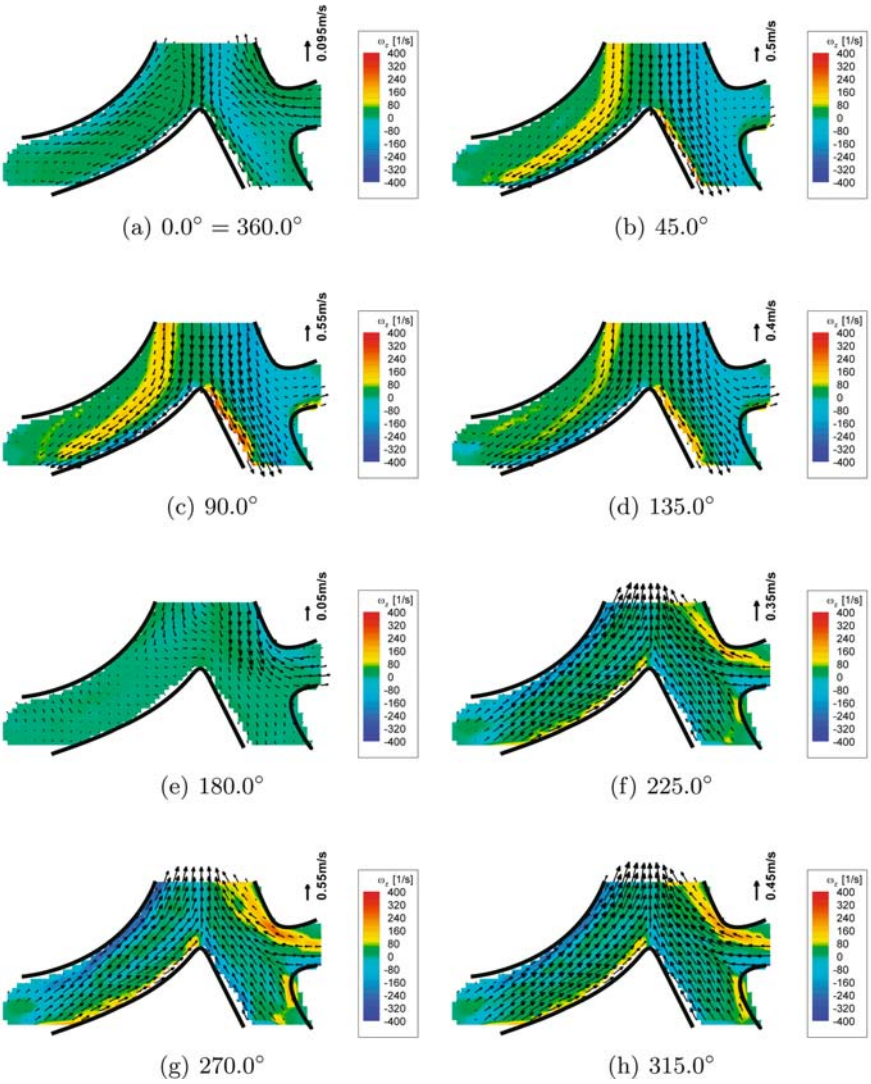


**Fig. 11.** Temporal evolution of the vorticity at different phase angles of the volumetric flow rate. Dorsal view. Vector plot of the local velocities. Only every second vector is displayed. Contours represent the local vorticity. Inspiration: (**b**–**d**), expiration: (**f**–**h**), almost no flow: (**a**, **e**)

bution, e.g., on the basis of stereoscopic PIV measurements. Furthermore, the investigation of the oscillating lung flow indicated the vortical flow regions to strongly change in shape and size due to the local acceleration of the flow for low Reynolds numbers, or in other words, due to the time dependence of the velocity. At expiration, the unsteady and steady flow solutions are more similar than at inspiration since hardly any secondary flow structures are observed.

Further measurements in subsequent generations of the lung geometry will be used to analyze to what extent the upstream flow conditions have an impact on the flow field in corresponding subbranches as a function of the local Reynolds number.

Additionally, a more realistic flow should be examined by incorporating the laryngeal region of the upper human airways in the model such that the flow entering the lung will have experienced likewise upstream conditions as the real human lung flow. Furthermore, it has to be investigated whether or not a defined pressure distribution at the end of the 6th generations' branches and controlled flow volumes for each of these branches possess an influence on the flow field of the upper airways.

Finally, the flow field during high-frequency oscillatory ventilation (HFV) with ventilation frequencies between 5 and 15 Hz will be investigated, since this technique has reached increasing clinical application. It is still to be investigated whether or not a variation of the Womersley number influences the flow structures in the lung for inspiration and expiration.

## References

[1] J. K. Comer, C. Kleinstreuer, S. Hyun, C. S. Kim: Aerosol transport and deposition in sequentially bifurcating airways, J. Biomech. Eng.-T ASME **122**, 152–158 (2000) 36, 37

[2] J. K. Comer, C. Kleinstreuer, C. S. Kim: Flow structures and particle deposition patterns in double-bifurcation airway models. Part 2. Aerosol transport and deposition, J. Fluid Mech. **435**, 55–80 (2001) 36, 37

[3] J. K. Comer, C. Kleinstreuer, Z. Zhang: Flow structures and particle deposition patterns in double-bifurcation airway models. Part 1. Air flow fields, J. Fluid Mech. **435**, 25–54 (2001) 36, 37

[4] T. Martonen: Commentary "Effects of asymmetric branch flow rates on aerosol deposition in bifurcating airways", by Z. Zhang, C. Kleinstreuer and C. S. Kim, J. Med. Eng. Technol. **25**, 124–126 (2001) 36

[5] S. Mochzuki: Convective mass transport during ventilation in a model of branched airways of human lungs, in *Proc. 4th Pacific Symposium on Flow Visualization and Image Processing (PSFVIP4)* (2003) 36

[6] R. C. Schroter, M. F. Sudlow: Flow patterns in models of the human bronchial airways, Resp. Physiol. **7**, 341–355 (1969) 36

[7] T. B. Martonen, X. Guan, R. M. Schreck: Fluid dynamics in airway bifurcations: II. secondary currents, Inhal. Toxicil. **13**, 281–289 (2001) 36

[8] J. B. Grotberg: Respiratory fluid mechanics and transport Processes, Annu. Rev. Biomed. Eng. **3**, 421–457 (2001) 36
[9] Y. Liu, R. M. C. So, C. H. Zhang: Modeling the bifurcating flow in an asymmetric human lung airway, J. Biomech. **36**, 951–959 (2003) 36, 37
[10] X. L. Yang, Y. Liu, R. M. C. So, J. M. Yang: The effect of inlet velocity profile on the bifurcation COPD airway flow, Comput. Biol. Med. **36**, 181–194 (2006) 36, 39
[11] A. Ramuzat, M. L. Riethmuller: PIV investigation of oscillating flows within a 3D lung multiple bifurcations model, in *Proc. 11th Int. Symp. on Applications of Laser Techniques to Fluid Mechanics* (2002) pp. 19.1.1–19.1.10 36
[12] F. Y. Leong, K. A. Smith, C.-H. Wang: Transport of Sub-micron Aerosols in Bifurcations, Molecular Engineering of Biological and Chemical Systems (MEBCS) (2005) 37
[13] R. J. Robinson, M. J. Oldham, R. E. Clinkenbeard, P. Rai: Experimental and numerical smoke carcinogen deposition in a multi-generation human replica tracheobronchial model, Ann. Biomed. Eng. **34**, 373–383 (2006) 37
[14] E. R. Weibel: *Morphometry of the Human Lung* (Springer, Berlin, Heidelberg 1963) 37
[15] C. G. Caro, R. C. Schroter, N. Watkins, S. J. Sherwin, V. Sauret: Steady inspiratory flow in planar and non-planar models of human bronchial airways, Proc. Roy. Soc. Lond. A **458**, 791–809 (2002) 37
[16] C. van Ertbruggen, C. Hirsch, M. Paiva: Anatomically based three-dimensional model of airways to simulate flow and particle transport using computational fluid dynamics, J. Appl. Physiol. **98**, 970–980 (2005) 37
[17] C. Brücker, W. Schröder: Flow visualization in a model of the bronchial tree in the human lung airways via 3-D PIV, in *Proc. of the 4th Pacific Symposium on Flow Visualization and Image Processing (PSFVIP4)* (2003) 37